Helium plasma implantation on metals: Nanostructure formation and visible-light photocatalytic response

Shin Kajita, Tomoko Yoshida, Daiki Kitaoka, Reo Etoh, Miyuki Yajima, Noriyasu Ohno, Hisao Yoshida,
Naoaki Yoshida, and Yoshitaka Terao

View Online   **Export Citation**   **CrossMark**

ARTICLES YOU MAY BE INTERESTED IN

Nanostructuring of molybdenum and tungsten surfaces by low-energy helium ions
Journal of Vacuum Science & Technology A **30**, 041306 (2012); https://doi.org/10.1116/1.4731196

 Comparison between helium plasma induced surface structures in group 5 (Nb, Ta) and group
6 elements (Mo, W)
Journal of Applied Physics **121**, 155301 (2017); https://doi.org/10.1063/1.4981128

Helium bubble bursting in tungsten
Journal of Applied Physics **114**, 243518 (2013); https://doi.org/10.1063/1.4860315

CrossMark
click for updates
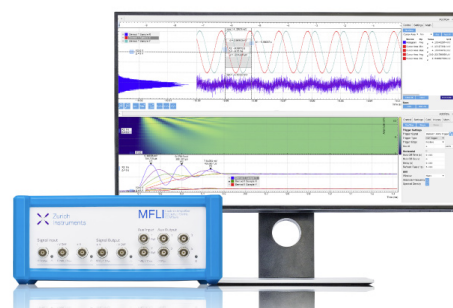
Helium plasma implantation on metals: Nanostructure formation and visible-light photocatalytic response

Shin Kajita,[1] Tomoko Yoshida,[1] Daiki Kitaoka,[2] Reo Etoh,[2] Miyuki Yajima,[2] Noriyasu Ohno,[2] Hisao Yoshida,[2] Naoaki Yoshida,[3] and Yoshitaka Terao[4]

[1]*EcoTopia Science Institute, Nagoya University, Nagoya 464-8603, Japan*
[2]*Graduate School of Engineering, Nagoya University, Nagoya 464-8603, Japan*
[3]*Research Institute for Applied Mechanics, Kyushu University, Fukuoka 816-8580, Japan*
[4]*Samsung Yokohama Research Institute, Japan*

It has been found recently that low-energy helium (He) plasma irradiation to tungsten (W) leads to the growth of W nanostructures on the surface. The process to grow the nanostructure is identified as a self-growth process of He bubbles and has a potential to open up a new plasma processing method. Here, we show that the metallic nanostructure formation process by the exposure to He plasma can occur in various metals such as, titanium, nickel, iron, and so on. When the irradiation conditions alter, the metallic cone arrays including nanobubbles inside are formed on the surface. Different from W cases, other processes than growth of fiberform structure, i.e., physical sputtering and the growth of large He bubbles, can be dominant on other metals during irradiation; various surface morphology changes can occur. The nanostructured W, part of which was oxidized, has revealed a significant photocatalytic activity under visible light (wavelength >700 nm) in decolorization of methylene blue without any co-catalyst. © *2013 American Institute of Physics.* [http://dx.doi.org/10.1063/1.4798597]

I. INTRODUCTION

In the course of the plasma surface interaction studies for nuclear fusion, it has been unexpectedly found in the mid 2000 that fiberform nanostructured tungsten (W), so-called "tungsten fuzz," is formed on W surface by helium (He) plasma irradiation.[1] In future fusion reactors including ITER, because W will be exposed to He ions under the formation conditions of the nanostructures, which was revealed experimentally,[2] the formation of the nanostructure has been attracting great interests in the field. Extensive investigations have been conducted to reveal the growth properties, formation conditions and mechanisms,[2–5] and changes in thermophysical property[6] and optical properties.[7,8]

Although the process of the nanostructure growth is identified to be related with a novel self-growth process of He bubbles,[3,4,7] the growth mechanism has not been entirely understood yet; the mechanisms are being investigated from experimental, theoretical, and numerical points of view. One of the interests related with the process is whether the nanostructure growth occurs on other metals. The growth of fiberform nanostructures has been reported only on W and Mo,[9,10] but the effects on other metals with lower melting points have not been investigated yet. Despite the fact that the unforeseen changes in optical and physical properties might be unwelcome in nuclear fusion reactors, they have a potential to be used for application fields.[7]

From application point of view, nanostructured materials are receiving attentions more and more due mainly to their distinctive optical, electrical, magnetic, and mechanical properties. Nanostructured metallic building has potentials to apply in various fields, such as solar absorber,[7]

catalysis[11] sensors,[11] fuel cells,[12] and so on. Concerning catalytic nanostructures, the importance is in its porosity, and three dimensional porosity is preferable compared with one-dimensional porosity like array of tubes.[13] Mesoporous metals (pre size 2-50 nm) are classified basically to aerogels,[13] nanoporous metals made by dealloying,[14] and nanotubular mesoporous materials by using special templates.[15,16] Since the He irradiated W has a larger effective surface area and complicated structure with high porosity, e.g., ~ 0.9,[17,18] it is thought that the material may be eligible catalytic material.

In this paper, the morphology changes due to He plasma irradiation to various metals are shown in Sec. II, and photocatalytic experiments are presented in Sec. III. Conclusions are given in Sec. IV. As for irradiation experiments, we conduct He irradiation to titanium (Ti), nickel (Ni), iron (Fe), and stainless steel (SS) and show the morphology changes in nanometer scale. The nanostructures are observed with a scanning electron microscope (SEM) and transmission electron microscope (TEM). On Ti and Fe, nanocone arrays are formed on the surface and the optical absorptivity of the blacken surface is measured. The processes that cause the morphology changes will be discussed. In Sec. III, characterization of W exposed He plasma is done by TEM and X-ray photoelectron spectroscopy (XPS). Photocatalytic experiments to decolorize methylene blue (MB) are conducted using the W nanostructure that was partially oxidized in air atmosphere. Interestingly, it is shown that the nanostructured W fabricated under He plasma irradiation exhibits a significant photocatalytic activity for visible light even at the wavelength longer than 700 nm without any co-catalysts.

II. HE IRRADIATION EXPERIMENTS

A. Setup

He plasma irradiation was conducted in the linear plasma devices NAGDIS-II (Nagoya Divertor Simulator). A schematic of the experimental setup is shown in Fig. 1. Details of the device can be found in Refs. 19 and 20. The plasma was produced by a direct current (DC) arc discharge using a heated LaB_6 cathode with discharge gas of He. A magnetic field, which is produced by solenoidal coils, is applied to suppress the diffusion of the plasma and a cylindrical plasma is formed. The strength of the magnetic field is ~0.1 T. The typical electron density and temperature of the He plasma are $10^{19} m^{-3}$ and 5 eV, respectively. Specimens were installed to the vacuum vessel and negatively biased electrically; the incident ion energy was typically 50–100 eV. The surface is heated by the plasma bombardment and the surface temperature is increased to above 1000 K without any cooling system. A water cooling stage is used when necessary to sustain the temperature sufficiently low. The surface temperature was measured by a radiation pyrometer before morphology change took place with the optical emittance of bulk material. The uncertainty in the temperature measurement could arise from the ambiguity in the optical emittance. For example, if the optical emittance had an ambiguity of 10% for Ti at 800 K, the uncertainty would be ±10 K.

B. Nanocone formation on Ti and SS

Figures 2(a) and 2(b) are SEM micrographs of Ti and SS samples, respectively, exposed to the He plasma. The surface temperature was approximately 550 K and the incident ion energy and He fluence are 75 eV and $6.4 \times 10^{25} m^{-2}$, respectively. Interestingly, nanocone array was formed on the surface by the He irradiation. It is thought that, different from W, He irradiation to these metals gives rise to physical sputtering, and leads to different morphology changes under slightly different irradiation condition. In Figs. 3(a) and 3(b), TEM micrographs of the Ti and SS samples cut with focused ion beam (FIB) milling process are also shown. The structure of Ti and SS is similar and the tips of the nanocones are very fine. The height of the Ti cone was approximately ~600 nm
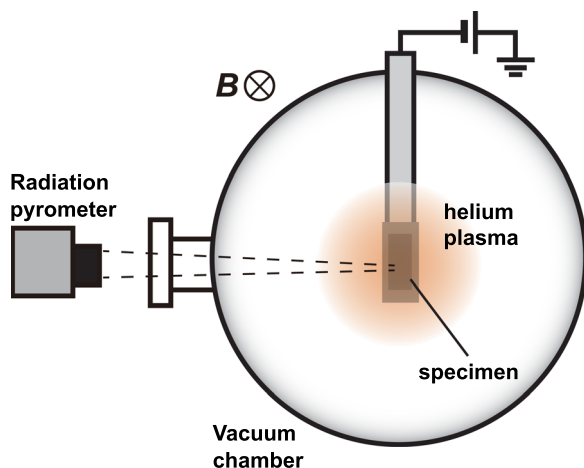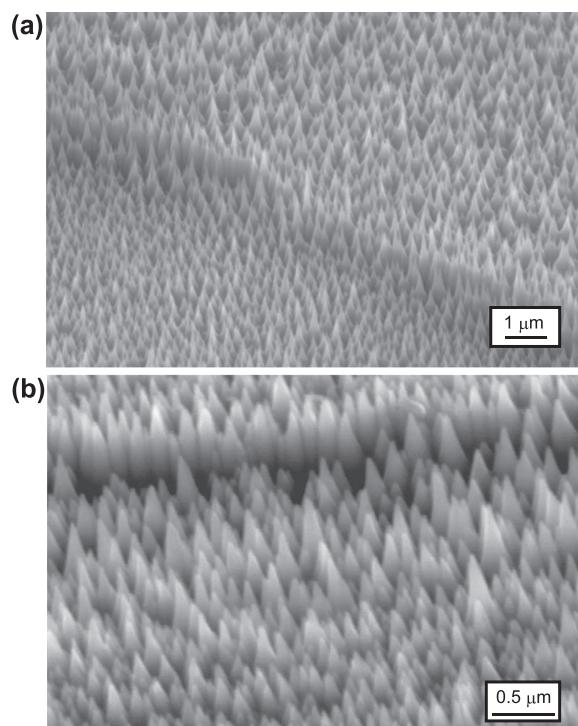
FIG. 2. (a) and (b) are the SEM micrographs of the Ti and SS samples, respectively, exposed to the helium plasma. Nanocones are formed on the surface. The surface temperature was approximately 550 K and the incident ion energy and helium fluence are 75 eV and $6.4 \times 10^{25} m^{-2}$, respectively.

and the bottom width was ~300 nm; the aspect ratio of a cone was approximately two. Especially on Ti cone, many He bubbles were observed inside the cones. He bubbles were also observed on SS cones, but it seemed that the number of bubbles was less than that on Ti cones.

The surface exposed to the He plasma became visually black. As indicated from the calculation of absorptivity for W pyramids,[21] cone shaped metal would be a good solar absorber. Figure 4(a) shows the setup for the hemispherical reflectance measurement. A linear polarized He-Ne laser at the wavelength of 633 nm irradiated the sample and the reflected light was collected by an integrating sphere. The polarization was changed by using $\lambda/2$ wavelength plate and a polarizing beam splitter. Figures 4(b) and 4(c) show total reflectances of the Ti and SS samples for the s and p polarizations, respectively. Before He irradiation, the reflectance at the normal incident angle was approximately 50%-60%, which was consistent with the values in an optical database. On the other hand, the optical reflectance significantly decreased by the He irradiation. At the normal incident angle, the reflectance was ~5% for both Ti and SS, showing that the reflectance decreases by an order of magnitude. Before irradiation, the reflectance increases with angle for p polarization, while it decreases with angle. The dependences agree well with the theoretical dependences.[22] On the other hand, after the irradiation, the dependence cannot be consistent with the theoretical dependence. Both for p and s polarizations, it increases with incident angle if the angle exceeds 40°. For s polarization, decreasing dependence remains around the normal incident in the case of SS.
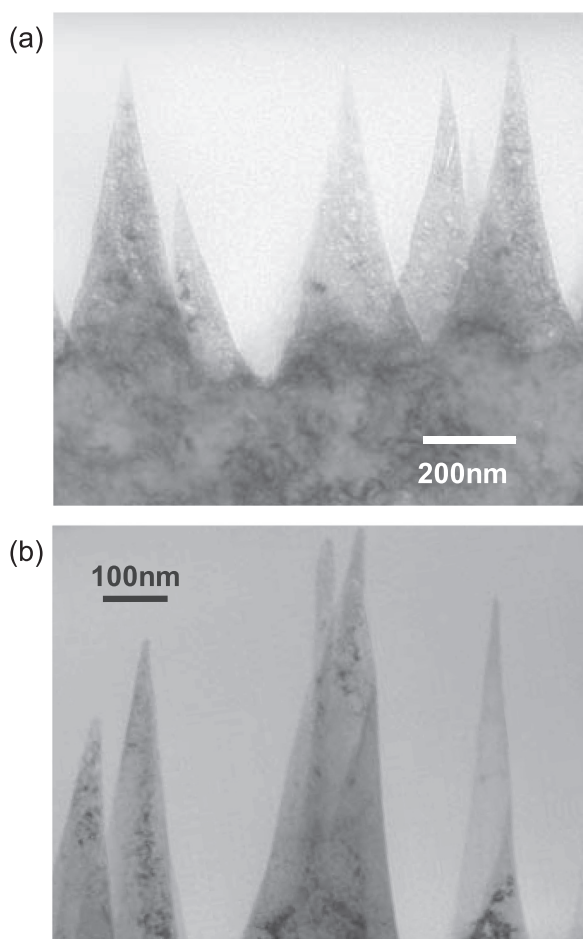
FIG. 1. A schematic of the experimental setup. Specimens are exposed to He plasmas in the linear plasma device NAGDIS-II.

FIG. 3. (a) and (b) are the TEM micrographs of the Ti and SS samples, respectively, exposed to the helium plasma.
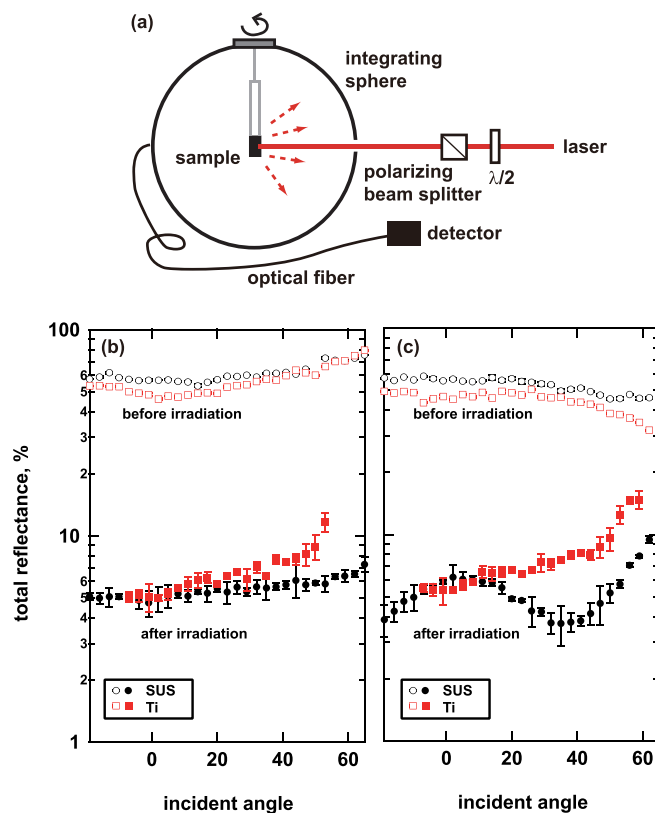

FIG. 4. (a) The setup for total reflectance measurement system. (b) and (c) The angular dependences of the total reflectance of Ti and SS specimens for p and s polarizations, respectively. Open and closed markers correspond to the reflectance before and after the helium irradiation, respectively.

The cone formation has been observed on metals irradiated by ion beams.[23,24] In those cases, seed atoms were inevitable;[25] the seed atoms led to the formation of protuberance on the surface, and sputtering and surface diffusion played an essential role to develop the cone growth.[26] In the present study, however, though the holder of the sample was made of Mo, it is doubtful that seed metal worked for the development, since the ion bombardment energy was so low that sputtering yield for Mo was negligibly small.[27] In conventional cone growth with seed atoms, the size of the cone is usually larger than 1 μm, and the cones are isolated from each other and distributed non-uniformly. On the other hand, the size of the cone in this study was smaller, say several hundreds of nanometers and the cones are distributed uniformly on the surface; the growth mechanism might be different.

Figure 5(a) presents a picture of He irradiated Ti samples. The area exposed to He plasma became black. Figure 5(b) presents a SEM micrograph of the boundary region between irradiated and non-irradiated areas on Ti sample. In the boundary region, surface becomes rough with protuberances probably because of helium bubbles underneath, in the similar manner as in the helium irradiated molybdenum surface.[28] In cases of cone formation by He plasma irradiation, protuberances formed by the helium bubbles may play a similar role that seed impurity had played conventionally.

C. Fiberform nanostructure formation on Ni, Fe, and Ti

Figures 6(a)–6(c) are SEM micrographs of Ti, Ni, and Fe exposed to the helium plasma, respectively. It is seen that metallic nanostructure similar to tungsten nanostructures is formed on the surfaces. The irradiated surface temperature was 800 K for Ti and 900 K for Fe. For Ni, the surface temperature was less than 800 K. It is recognized that the growth rate of helium bubbles can be organized with the normalized surface temperature to the melting point.[29] Since the melting points of Ti, Ni, and Fe are much lower than that of W, the
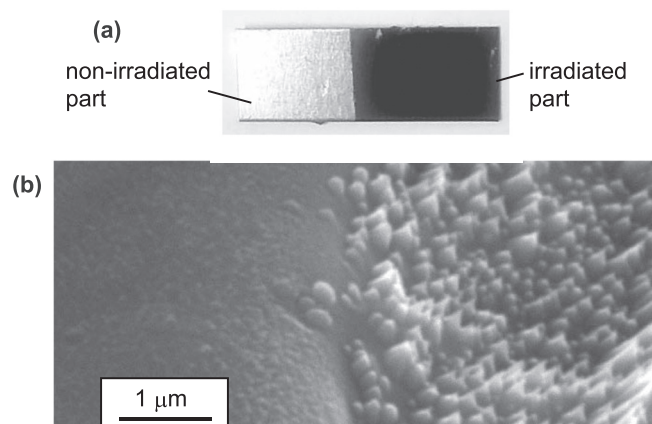

FIG. 5. (a) A picture of a He irradiated Ti. (b) A SEM micrograph of the boundary region between irradiated and non-irradiated areas on the Ti sample.
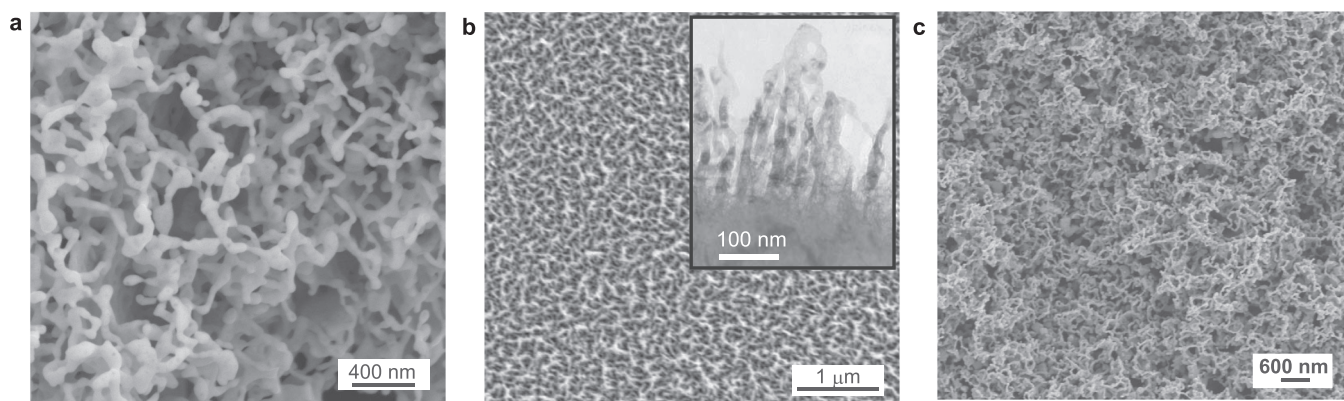
FIG. 6. SEM micrographs of (a) Ti, (b) Ni, and (c) Fe exposed to the helium plasmas.

irradiation was conducted at the surface temperature lower than threshold temperature of $\sim 1000\,K$ for W nanostructure formation.[2] The experiments were conducted at temperatures lower than $1000\,K$, and the difference in the temperature between metals did not have significant meaning here. The incident ion energy was $70\,eV$ for Ti, $80\,eV$ for Ni, and $82\,eV$ for Fe, and the helium fluence was $5.5 \times 10^{25}\,m^{-2}$ for Ti, $1.0 \times 10^{26}\,m^{-2}$ for Ni, and $3.9 \times 10^{26}\,m^{-2}$ for Fe. In Fig. 6(b), a cross-sectional TEM micrograph of the helium irradiated Ni is shown. A thin sample was prepared with a FIB milling process and the TEM micrograph was taken. It is seen that the thickness of the nanostructured layer was 200-300 nm, and the bubbles are observed in the structures in the similar manner as the helium bubbles in W.

It has been revealed from the experiments of nanostructured tungsten that the growth rate of nanostructured layer is proportional to the square root of helium fluence.[3] The growth rate was also dependent on the surface temperature[3] and the incident ion energy.[30] Typically, when the fluence was $10^{26}\,m^{-2}$, the corresponding thickness of the nanostructured layer will be approximately $1.5\,\mu m$ for tungsten case at the surface temperature of $1400\,K$ and the incident ion energy of $50\,eV$.[4] Thus, it can be said that the thickness of the layer of Ni shown in Fig. 6(b) was considerably thinner compared with the case of tungsten; the growth rate should be lower than that of tungsten under the present condition. The formation of helium bubbles and the coalescence behavior in Ni might be different from tungsten. Moreover, sputtering might have played a role to make the growth rate low.

Still, it is highly likely that these nanostructures are developed on the surface in the same processes as the tungsten nanostructure.[2,4] The helium particles impinged on the surface are diffused into the material. Then, bubbles packed with highly pressurized helium are formed, and consequently, the surface is distorted by the pressure of helium bubbles and some bubbles make holes when they intersect the surface. On increasing the helium fluence, the structure becomes finer and longer, and network fiberform nanostructures fully cover the surface.

D. Various nanostructures on Ti

He irradiation experiments on Ti under various conditions revealed that complicated nanostructures can be formed by He plasma irradiation. Figures 7(a) and 7(b) present TEM micrographs of He irradiated Ti with different magnifications. He irradiation was conducted at the surface temperature of $850\,K$ and incident ion energy of $73\,eV$ up to the He fluence of $2.6 \times 10^{25}\,m^{-2}$. Large holes are formed near the surface and cones are formed on the top of the structures. There were many small bubbles below the holes. The structure seemed very fragile; some parts might have been removed from the surface during the irradiation. It is likely that the large holes with the size of 100–300 nm were grown from much smaller He bubbles. The shape of large bubbles seen in Fig. 7(a) had polygon structure similar to the ones observed on tungsten when the surface temperature was rather high ($\sim 1800\,K$).[4] When helium gas is packed at the equilibrium pressure in bubbles, the shape should be spherical. Polygon shape indicated that the inner pressure of the bubble was considerably lower than the equilibrium pressure.

Similar to the case of tungsten, the incident ion energy and the surface temperature seem to be the important parameters to determine the surface morphology change. One of the differences from tungsten case is that the sputtering could become significant even in this low energy range. It is of importance for future work to investigate the relationship between the experimental condition and morphology change thoroughly by systematically changing the experimental conditions. In cases of W and Mo, it is thought that He plasma irradiation does not increase the surface temperature enough to significantly promote the growth of He bubbles. This is because the growth rate of helium bubbles can be roughly characterized with the temperature normalized to melting point[29] and those of W and Mo are relatively high. Without cooling system, the temperature of samples is increased by plasma bombardment and can be higher than $1000\,K$ easily in our device. Such a temperature will be suitable to nanostructure formation for W and Mo, but the temperature should be too high for other metals such as Ti, Ni, which have lower melting points, to sustain the fiberform nanostructures. Thus, sufficient cooling to sustain appropriate temperature is necessary if fiberform nanostructure formation was desired.

Moreover, different from W and Mo, significant sputtering occurs and sputtering can dominate the surface morphology change compared with the nanostructure growth. Therefore, compared with W and Mo, it may be slightly harder to seek appropriate irradiation conditions for fiberform
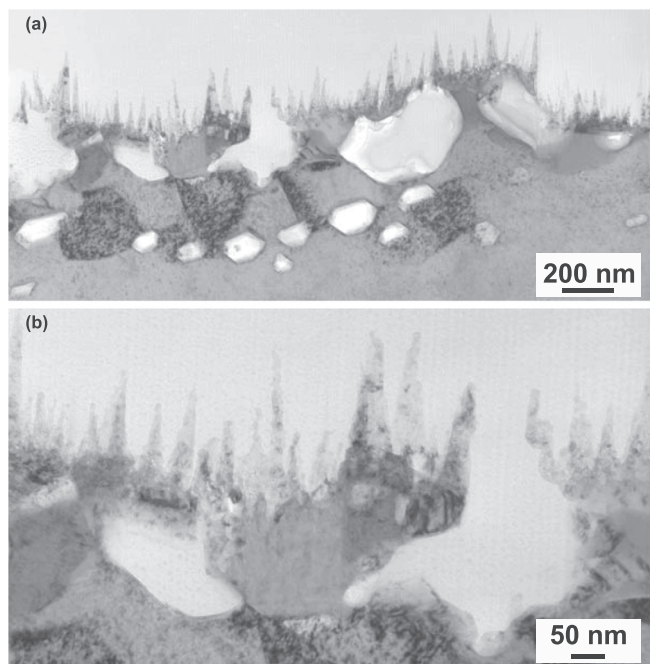
FIG. 7. (a) and (b) TEM micrographs of Ti exposed to He plasma at the surface temperature of 850 K and the incident ion energy of 73 eV with the He fluence of 2.6×10^{25} m^{-2}.

nanostructure formation on other metals, which have a low melting point and low sputtering threshold energy.

Conversely, by choosing appropriate conditions in terms of surface temperature and incident ion energy, the suitable surface morphology change can be selected from fiberform nanostructure surface, nanocone array, a surface with helium bubbles, or complicated structures mixed with them. In this study, though a detailed survey about the relations between the irradiation condition and various morphology change is not presented, it will be of interest to investigate them thoroughly in experiments on various metals.

III. VISIBLE LIGHT PHOTOCATALYTIC ACTIVITY

A. Characterization of W nanostructure

Figure 8(a) is a SEM micrograph of a typical W exposed to He plasma. The He fluence was 2.4×10^{25} m^{-2}. It is noted that the incident ion energy was less than 100 eV, which is lower than the displacement energy of W atoms and threshold energy of physical sputtering. It is seen that the fiberform nanostructures are grown from the surface with the thickness of $\sim$700 nm. It has been revealed that fiberform nanostructures can be formed in the temperature range of 1000–2000 K when the incident ion energy is greater than 20–30 eV. Typical He fluence necessary to form the nanostructure is $\sim 10^{25}$ m^{-2}, and the layer thickness increases with the square root of He fluence.[3]

Figure 8(b) shows TEM micrographs of He irradiated W specimens. The irradiation conditions were slightly different from that in Fig. 8(a), but the similar structure was formed when the above conditions are satisfied. The surface temperature was 1400 K and the He fluence was 5.4×10^{25} m^{-2}. In Fig. 8(b), helium bubbles inside the structure are clearly observed. The width of the structure
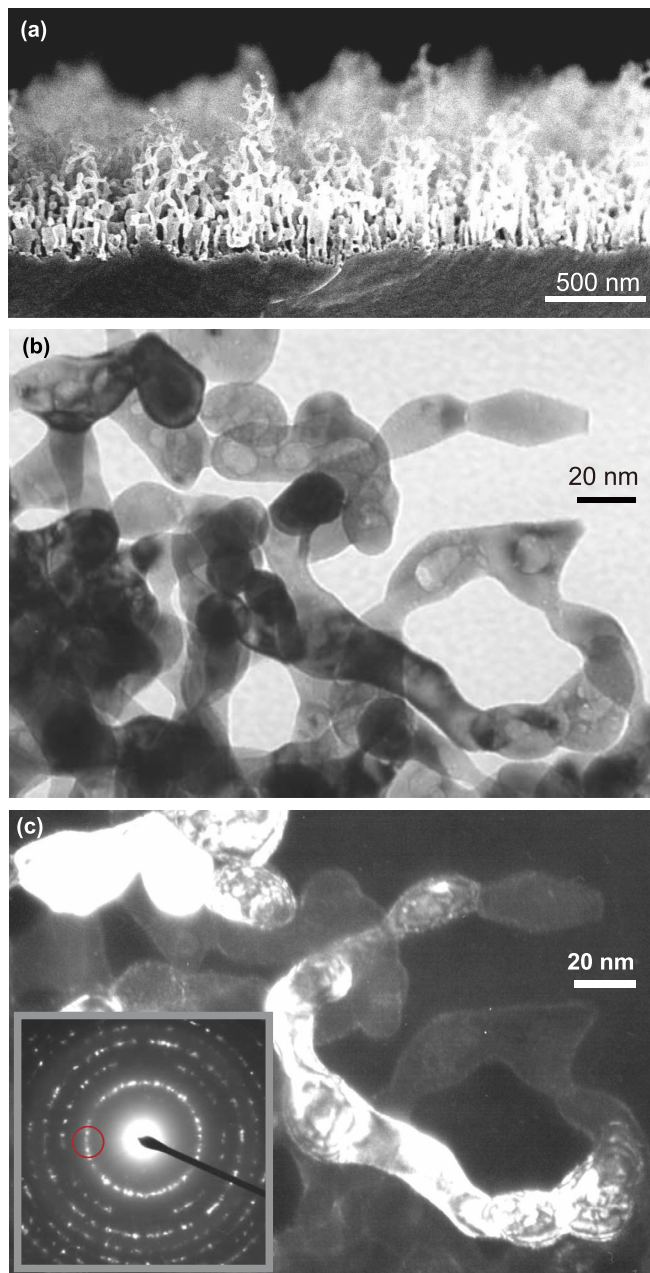

FIG. 8. (a) A SEM micrograph of W exposed to He plasma. (b) and (c) TEM micrographs of W exposed to He plasma. (b) is a bright field image and (c) is a dark field image.

was approximately 20 nm. Moreover, He bubbles with the size of $\sim$10 nm exist in many places inside the structure. In addition to rather large bubbles, many smaller bubbles, the size of several nm, are seen in the structure. Figure 8(c) presents a dark field image of the nanostructured W shown in Fig. 8(b). From a diffraction pattern, shown in the inset of Fig. 8(c), it is seen that the structure is primarily composed of W, but there is a thin layer composed of clusters of fine crystal grains with the thickness of $\sim$1 nm.

Shown in Fig. 9(a) are XPS spectra of the nanostructured W and commercial WO$_3$ powder. The irradiation was conducted at the surface temperature of 1300 K and the incident ion energy of 70 eV up to the He fluence was 2×10^{25} m^{-2}. (The difference in the irradiation conditions does not affect
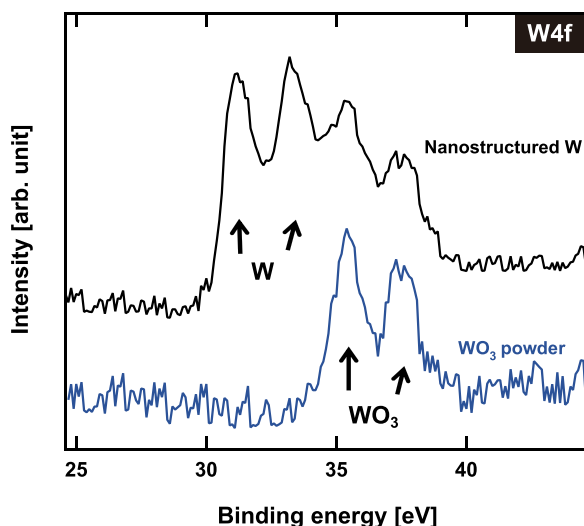
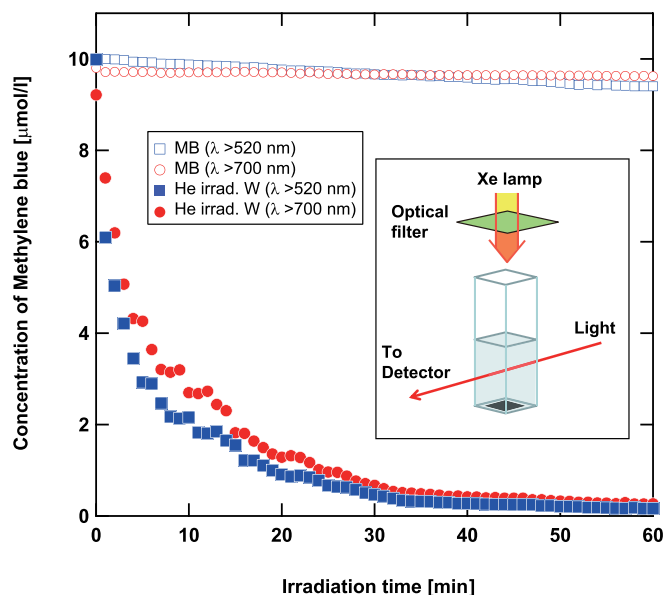FIG. 9. XPS spectra for the nanostructured tungsten and WO_3 powder.

FIG. 10. Time courses of MB decolorization over the tungsten samples exposed to helium plasma. The edge wavelengths of the used longpass filters were 520 (square) and 700 nm (circle).

the properties of material.) There were peaks of WO_3 ($W4f_{5/2}$ and $W4f_{7/2}$) around 35.5 and 37.6 eV for both samples, while W peaks at 30.8 and 33.0 eV can only be found on the nanostructured W. The surface of the nanostructured W was oxidized during being exposed to air after the plasma irradiation. It was observed in Fig. 8(c) that there was a thin layer on the surface with the thickness of 1 nm. Considering the fact that XPS spectra have strong WO_3 peaks, it is likely that the layer corresponds to WO_3 clusters.

B. Methylene blue decolorization

A typical photocatalytic experiment was conducted using the setup shown in the inset of Fig. 10. The W sample ($8 \times 8 \times 0.3$ mm^3) was placed in 2 ml of aqueous MB ($C_{16}H_{18}N_3SCl$) solution (10 μmol/l) and exposed to visible-light from a 300 W Xe lamp through an optical filter. Two longpass optical filters with the edge wavelengths of 520 and 700 nm were used. Figure 10 shows the time courses of the concentration of MB with and without the nanostructured W sample. Without the sample, the concentration of MB did not change. Also, we have confirmed that the MB decolorization was negligible over the commercial WO_3 powder sample. On the other hand, the MB decolorization proceeded over the sample and monotonically decreased with the irradiation time even if the edge wavelength of the filter was 700 nm, which is almost the nominal red edge of visible light. When MB is dissolved in water, the solution becomes blue. Although it is still not clear whether MB was decomposed, it is highly likely that MB was reduced to leuko-methylene blue, which is colorless.

The thickness of the layer of WO_3 can be identified to be typically ~1 nm from the TEM micrograph. However, the surface might not be totally covered with WO_3. An experiment was conducted using nanostructure tungsten oxidized at 473 K for 30 min in air atmosphere. Interestingly, the photocatalytic response was degraded by the oxidization process at an elevated temperature compared with the sample oxidized at room temperature. Thus, we suspect that WO_3 might not fully cover the surface when the sample was oxidized

spontaneously, and mixture of W and WO_3 surfaces may play a significant role to enhance the visible light photocatalytic response.

Note that a photocatalytic process cannot usually proceed over WO_3 under those light irradiation, since the band gap energy of WO_3 is 2.5 eV, which is greater than the photon energies. The results indicate that an interesting reaction that does not occur on conventional WO_3 proceeds over the nanostructured W. The oxidized tungsten has been paid attention as a prominent photocatalytic material working with a visible light, since the band gap is 2.5 eV, less than that of titanium oxide. Recently, there were many attempts to utilize WO_3 for the decomposition of organic matters with support catalyst such as Pt, Pd, CuO, and so on.[31–33] One of the significant differences from those studies is that the visible light photocatalytic activity appeared without any support catalyst in this study.

It was recognized that surface effect would be enhanced when the size of the structure was smaller than 10 nm.[34] There is a possibility that the inner porous structure by helium bubbles can enhance the surface effect. In other words, the thickness of the lid of the helium bubbles can be less than 10 nm when the helium bubbles are formed inside the structure, though the structure itself is in mesoscopic scale. Another possibility is that the nanostructured material has new energy states and transitions between those states exhibit the fascinating photocatalytic property. Also, similar to the one recently reported on gold on TiO_2 surfaces,[35] local surface plasmon resonance might be excited on the surface. The understanding of the mechanism and investigation of photocatalytic activity on other reactions are currently underway.

IV. CONCLUSIONS

Helium plasma irradiations were conducted in various metals, such as titanium (Ti), nickel (Ni), iron (Fe), and SS.

On Ti and SS, nanocone arrays were formed on the surface under some condition when the surface temperature was low, i.e., 550 K. Angular dependence of optical absorptances for p and s polarizations was measured at 633 nm with a laser and an integrating sphere. It was found that the optical reflectance decreased by an order of magnitude for both SS and Ti surfaces. Different from bulk materials, the optical reflectance increases with the incident angle for both s and p polarized lights. When the surface temperature was slightly higher (e.g., 800–900 K), fiberform nanostructures were observed on the surfaces of Ti, Ni, and Fe. When the surface temperature was raised to 850 K, the Ti surface had large bubbles (200–300 nm) and nanocones.

Although no systematic survey to reveal the conditional areas to form each structure was conducted in this study, physical sputtering and the growth of He bubbles can be dominant process for the morphology change, different from tungsten (W) and molybdenum (Mo). If we can identify the relation between the condition and types of morphology changes, He plasma irradiation to metals will be useful tool to develop nanostructures on metal surface. Different from silicon and carbon, for which plasma processing technique has been a versatile nanofabrication tool,[36] plasmas have played a limited role for metals. The present study would give a hope that He plasma implantation on metals could be a new fabrication tool for nanometer sized metallic structures.

He irradiated nanostructured W was analyzed by transmission electron microscopy. From a dark field image, it was found that there was a thin layer on surface less than 1 nm. X-ray photoelectron spectroscopy observed W and WO_3 peaks on the nanostructure. It was thought that part of the surface was oxidized in air atmosphere. Photocatalytic experiments were conducted using the nanostructured W to decolorize methylene blue. Significant decolorization occurred on the nanostructure W for visible light. The decolorization proceeded even for the light of which the wavelength was >700 nm. Although the mechanism of the process is yet to be understood, it is a surprising fact that the photon energy was significantly lower than the normal WO_3 band gap energy of 2.5 eV. In future, it is of interest to further explore the potential impact of the helium irradiated nanostructured metals as a catalytic material using different reaction processes and metals other than W.

ACKNOWLEDGMENTS

[1]S. Takamura, N. Ohno, D. Nishijima, and S. Kajita, Plasma Fusion Res. **1**, 051 (2006).
[2]S. Kajita, W. Sakaguchi, N. Ohno, N. Yoshida, and T. Saeki, Nucl. Fusion **49**, 095005 (2009).
[3]M. Baldwin and R. Doerner, Nucl. Fusion **48**, 035001 (2008).
[4]S. Kajita, N. Yoshida, R. Yoshihara, N. Ohno, and M. Yamagiwa, J. Nucl. Mater. **418**, 152 (2011).
[5]S. I. Krasheninnikov, Phys. Scr. **T145**, 014040 (2011).
[6]S. Kajita, S. Takamura, N. Ohno, D. Nishijima, H. Iwakiri, and N. Yoshida, Nucl. Fusion **47**, 1358 (2007).
[7]S. Kajita, T. Saeki, N. Yoshida, N. Ohno, and A. Iwamae, Appl. Phys. Express **3**, 085204 (2010).
[8]S. Kajita, T. Saeki, Y. Hirahata, and N. Ohno, Jpn. J. Appl. Phys., Part 1 **50**, 01AH02 (2011).
[9]S. Kajita, S. Takamura, and N. Ohno, Nucl. Fusion **49**, 032002 (2009).
[10]G. D. Temmerman, K. Bystrov, J. J. Zielinski, M. Balden, G. Matern, C. Arnas, and L. Marot, J. Vac. Sci. Technol. A **30**, 041306 (2012).
[11]S. Seal, *Functional Nanostructures: Processing, Characterization, and Applications* (Springer, New York, 2008).
[12]G. Wilde, *Nanostructured Materials* (Elsevier, Oxford, 2009).
[13]D. R. Rolison, Science **299**, 1698 (2003).
[14]J. Erlebacher, M. J. Aziz, A. Karma, N. Dimitrov, and K. Sieradzki, Nature **410**, 450 (2001).
[15]Y. Ding, A. Mathur, M. Chen, and J. Erlebacher, Angew. Chem., Int. Ed. **44**, 4002 (2005).
[16]T. Kijima, T. Yoshimura, M. Uota, T. Ikeda, D. Fujikawa, S. Mouri, and S. Uoyama, Angew. Chem., Int. Ed. **43**, 228 (2004).
[17]S. Kajita, N. Yoshida, R. Yoshihara, N. Ohno, T. Yokochi, M. Tokitani, and S. Takamura, J. Nucl. Mater. **421**, 22 (2012).
[18]D. Nishijima, M. Baldwin, R. Doerner, and J. Yu, J. Nucl. Mater. **415**, S96 (2011).
[19]N. Ohno, D. Nishijima, S. Takamura, Y. Uesugi, M. Motoyama, N. Hattori, H. Arakawa, N. Ezumia, S. Krasheninnikov, A. Pigarov, and U. Wenzel, Nucl. Fusion **41**, 1055 (2001).
[20]S. Kajita, D. Nishijima, N. Ohno, and S. Takamura, J. Appl. Phys. **100**, 103304 (2006).
[21]E. Rephaeli and S. Fan, Appl. Phys. Lett. **92**, 211107 (2008).
[22]J. F. Figueira and S. J. Thomas, IEEE J. Quantum Electron. **18**, 1381 (1982).
[23]A. D. G. Stewart and M. W. Thompson, J. Mater. Sci. **4**, 56 (1969).
[24]G. K. Wehner and D. J. Hajicek, J. Appl. Phys. **42**, 1145 (1971).
[25]G. K. Wehner, J. Vac. Sci. Technol. A **3**, 1821 (1985).
[26]L. Begrambekov, V. Telkovsky, and A. Zakharov, Nucl. Instrum. Methods Phys. Res. B **115**, 456 (1996).
[27]D. Rosenberg and G. K. Wehner, J. Appl. Phys. **33**, 1842 (1962).
[28]S. Kajita, T. Saeki, N. Ohno, M. Tokitani, T. Hatae, and W. Sakaguchi, J. Nucl. Mater. **417**, 838 (2011).
[29]J. H. Evans, J. Nucl. Mater. **334**, 40 (2004).
[30]W. Sakaguchi, S. Kajita, N. Ohno, and M. Takagi, J. Nucl. Mater. **390–391**, 1149 (2009).
[31]R. Abe, H. Takami, N. Murakami, and B. Ohtani, J. Am. Chem. Soc. **130**, 7780 (2008).
[32]T. Arai, M. Horiguchi, M. Yanagida, T. Gunji, H. Sugihara, and K. Sayama, Chem. Commun. **2008**, 5565.
[33]T. Arai, M. Yanagida, Y. Konishi, Y. Iwasaki, H. Sugihara, and K. Sayama, Catal. Commun. **9**, 1254 (2008).
[34]M. Haruta, Catal. Today **36**, 153 (1997).
[35]E. Kowalska, O. O. P. Mahaney, R. Abe, and B. Ohtani, Phys. Chem. Chem. Phys. **12**, 2344 (2010).
[36]K. Ostrikov, Rev. Mod. Phys. **77**, 489 (2005).